Inorganic Chemistry
Article

Inorg. Chem. **2009**, *48*, 11903–11908 **11903**
DOI: 10.1021/ic901930w

Ligand-Controlled Magnetic Interactions in Mn_4 Clusters

Erik Kampert, Femke F. B. J. Janssen, Danil W. Boukhvalov, Jaap C. Russcher, Jan M. M. Smits, René de Gelder, Bas de Bruin,*,† Peter C. M. Christianen, Uli Zeitler,* Mikhail I. Katsnelson, Jan C. Maan, and Alan E. Rowan*

Institute for Molecules and Materials, Radboud University Nijmegen, Toernooiveld 7, 6525 ED Nijmegen, The Netherlands. † Present address: Homogeneous and Supramolecular Catalysis, Van't Hoff Institute for Molecular Sciences, University of Amsterdam, 1018 WV Amsterdam, The Netherlands

Received October 1, 2009

A method is presented to design magnetic molecules in which the exchange interaction between adjacent metal ions is controlled by electron density withdrawal through their bridging ligands. We synthesized a novel Mn_4 cluster in which the choice of the bridging carboxylate ligands (acetate, benzoate, or trifluoroacetate) determines the type and strength of the three magnetic exchange couplings (J_1, J_2, and J_3) present between the metal ions. Experimentally measured magnetic moments in high magnetic fields show that, upon electron density withdrawal, the main antiferromagnetic exchange constant J_1 decreases from -2.2 K for the $[Mn_4(OAc)_4]$ cluster to -1.9 K for the $[Mn_4(H_5C_6COO)_4]$ cluster and -0.6 K for the $[Mn_4(F_3CCOO)_4]$ cluster, while J_2 decreases from -1.1 K to nearly 0 K and J_3 changes to a small ferromagnetic coupling. These experimental results are further supported with density-functional theory calculations based on the obtained crystallographic structures of the $[Mn_4(OAc)_4]$ and $[Mn_4(F_3CCOO)_4]$ clusters.

Introduction

Understanding and controlling magnetism on a molecular scale are key research topics of modern material science, with single-molecule magnets (SMMs) such as Mn_{12}, Fe_8, and V_{15} clusters as the most prominent examples.[1−3] The discovery of the magnetic molecular material Prussian Blue initiated this research field of molecular magnetism, and a wide variety of well-described compounds have been developed.[4] At first, the research was focused on magnetic molecule design, which evolved into the exploration of diverse physical properties of the obtained compounds as soon as the first single-molecule magnets were found.[5,6] In our studies, we have developed a new Mn_4 cluster whose magnetic properties can be readily modified in a modular fashion. Phenomenologically, the magnetic exchange interaction J between metal ions is determined by the overlap of electronic orbitals expressed in a series of symmetry rules.[7,8] Influencing the geometrical orbital overlap through structural modification of a magnetic molecule has indeed allowed a modification of its magnetic properties.[9] Alternatively, magnetic exchange interactions between ions can be tuned by a chemical modification of the molecule's backbone, thereby changing the overlap of the orbital wave functions between the magnetic ions by altering the electron-withdrawing properties of the ligands.[10]

We apply the concept of ligand-controlled magnetic interaction to design and synthesize new metal-organic magnetic molecules with exchangeable ligands defining their magnetic properties. By choosing the appropriate ligand, we can control the electron withdrawal from the metal ion core, thereby modifying the intramolecular exchange interactions. Specifically, we have synthesized Mn_4 clusters incorporating a pentadentate pyridine-diimine-type ligand (LH_2) with a chemical structure, as shown in Figure 1a.[11] A wide variety of carboxylates can be chosen to bridge the metal ions while the structure of the integral cluster remains intact. We use acetate and trifluoroacetate as bridging ligands, because of their large difference in electron density withdrawing character and similarity in size. In this way, the cluster's molecular structure remains practically unaffected, and the change in

*To whom correspondence should be addressed. E-mail: u.zeitler@science.ru.nl (U.Z.), b.debruin@uva.nl (B.d.B.), a.rowan@science.ru.nl (A.E.R.).

(1) Sessoli, R.; Gatteschi, D.; Caneschi, A.; Novak, M. A. *Nature* **1993**, *365*, 141.
(2) Sangregorio, C.; Ohm, T.; Paulsen, C.; Sessoli, R.; Gatteschi, D. *Phys. Rev. Lett.* **1997**, *78*, 4645.
(3) Gatteschi, D.; Pardi, L.; Barra, A. L.; Muller, A.; Doring, J. *Nature* **1991**, *354*, 463.
(4) Holden, A. N.; Matthias, B. T.; Anderson, P. W.; Lewis, H. W. *Phys. Rev.* **1956**, *102*, 1463.
(5) Gatteschi, D.; Sessoli, R. *Angew. Chem., Int. Ed.* **2003**, *42*, 268.
(6) Gatteschi, D.; Caneschi, A.; Pardi, L.; Sessoli, R. *Science* **1994**, *265*, 1054.
(7) Goodenough, J. B. *J. Phys. Chem. Solids* **1958**, *6*, 287.
(8) Kanamori, J. *J. Phys. Chem. Solids* **1959**, *10*, 87.
(9) Kahn, O. *Angew. Chem., Int. Ed.* **1985**, *24*, 834.
(10) Rodriguez-Fortea, A.; Alemany, P.; Alvarez, S.; Ruiz, E. *Chem.—Eur. J.* **2001**, *7*, 627.
(11) de Bruin, B.; Bill, E.; Bothe, E.; Weyhermuller, T.; Wieghardt, K. *Inorg. Chem.* **2000**, *39*, 2936.

Published on Web 11/16/2009

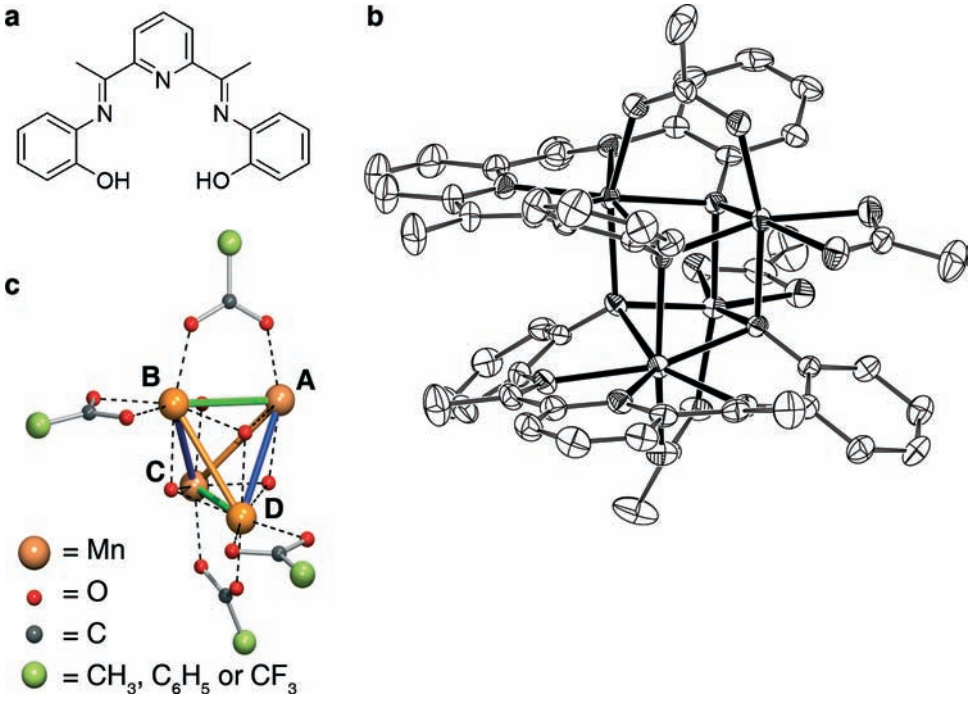

Figure 1. Structure of the manganese clusters. (a) Molecular structure of the pyridine-diimine-type ligand LH_2, occupying the equatorial positions in the Mn_4 clusters. (b) ORTEP representation of **1** with thermal ellipsoids set at 50% probability. The three DMF solvent molecules and hydrogen atoms are omitted for clarity. The crystal structure displays a cubic $[Mn_4O_4]$ core, with μ_3-bridging oxygen atoms provided by the four phenolate residues of the pyridine-diimine ligands, analogous for all three synthesized Mn_4 clusters. The clusters contain two pairs of equivalent Mn^{II} atoms, which are bridged by two carboxylate ligands, in this case acetate. The first set has a distorted pentagonal-bipyramidal geometry with L_2 occupying the equatorial positions, while the axial donors are a μ_3-oxygen from the other pyridine-diimine ligand and one oxygen of a μ_2-acetate. The second set displays distorted octahedral geometry with the two μ_3-oxygens and one chelating acetate in the equatorial plane and with one oxygen of the μ_2-acetate and a μ_3-oxygen in the axial positions. (c) Schematic representation of the distorted cubane-like core consisting of four manganese ions, four phenolate oxygens, and four carboxylate ligands (two chelating to B respectively D and two bridging A−B respectively C−D). Because of symmetry, there are three different exchange interaction paths between the ions J_1 (blue), J_2 (green), J_3 (red).

the magnetic character is only due to the electronic properties of the ligands. As an intermediate system, we have also investigated Mn_4 clusters with benzoate ligands, which have an electron density withdrawing character between that of acetate and that of trifluoroacetate.

For the synthesis of our Mn_4 cluster with acetate ligands, we reacted 2,6-diacetylpyridine with 2-aminophenol in the presence of 2 equiv of $Mn(OAc)_2 \cdot 4H_2O$, yielding a microcrystalline material containing the Mn_4 cluster **1** (see the Experimental Section). Recrystallization from dimethylformamide/pentane gave crystals suitable for X-ray diffraction. The crystal structure is shown Figure 1b with its $[Mn_4O_4]$ core schematically visualized in Figure 1c. The structure displays a cubic core, with μ_3-bridging oxygen atoms provided by the four phenolate residues of the pyridine-diimine ligands, two chelating acetates in the equatorial planes and two bridging acetates in the axial positions. The Mn−O and Mn−N bond lengths are in good agreement with the reported values for Mn^{II}−N and Mn^{II}−O distances and show unambiguously that the core of our cluster is formed by four Mn^{II} ions with five unpaired electrons per ion.[12] Interestingly, the cubic core structure resembles the water-oxidizing complex in photosystem II, which enables plants to oxidize water to dioxygen.[13] Previous research on photosystem II mimics has shown complicated magnetic behavior with both antiferromagnetic and ferromagnetic exchange interactions within the cluster.[14] Therefore, elucidating the magnetic properties of our specific Mn_4-based cluster and its variants with different carboxylate ligands may clarify the generic magnetic behavior of tetranuclear manganese clusters (such as photosystem II) in general.

Mn_4 cluster **2** was prepared by reacting $Mn(H_5C_6COO)_2 \cdot 2H_2O$ with 2,6-diacetylpyridine and 2-aminophenol. The addition of 5 equiv of trifluoroacetic acid to a solution of **1** in methanol yielded Mn_4 cluster **3** with four trifluoroacetate ligands. The $[Mn_4O_4]$ core, as depicted in Figure 1c, remains intact upon ligand variation; all modifications of the magnetic properties can be attributed to the influence of the ligands on the electronic orbitals alone. Details of the synthesis of these compounds can be found in the Experimental Section.

Magnetometry Results. For a full magnetic characterization of our three Mn_4 clusters with different ligands, we have measured the magnetization in terms of magnetic moment per cluster of three powdered samples at various temperatures in magnetic fields up to 31 T. The results for **1**, **2**, and **3** are shown in Figure 2a,b,c respectively; Figure 3 displays the low-temperature ($T = 4.2$ K) magnetic-moment isotherms for all three samples. All curves start with a finite slope and slowly approach saturation at the highest magnetic fields and the lowest

(12) Belal, A. A.; Fallis, I.; Farrugia, L. J.; Macdonald, N. M.; Peacock, R. D. *J. Chem. Soc., Chem. Commun.* **1991**, 402.
(13) Ferreira, K. N.; Iverson, T. M.; Maghlaoui, K.; Barber, J.; Iwata, S. *Science* **2004**, *303*, 1831.
(14) Hendrickson, D. N.; Christou, G.; Schmitt, E. A.; Libby, E.; Bashkin, J. S.; Wang, S. Y.; Tsai, H. L.; Vincent, J. B.; Boyd, P. D. W.; Huffman, J. C.; Folting, K.; Li, Q. Y.; Streib, W. E. *J. Am. Chem. Soc.* **1992**, *114*, 2455.

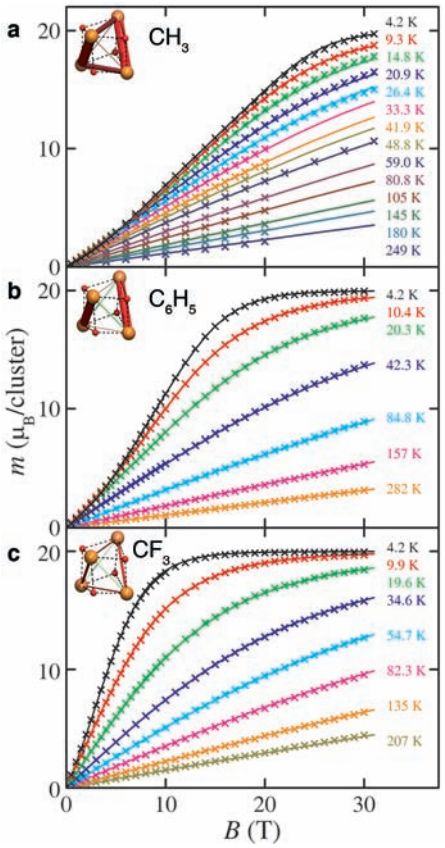

Figure 2. Magnetization of the individual manganese clusters. The measured magnetic moment isotherms all start at the nonmagnetic $S = 0$ state and show the consecutive population of higher spin energy levels upon a magnetic field increase. At the lowest temperatures and high magnetic fields, this results in the full population of the $S = 10$ state and saturation of the magnetization. The solid lines represent the best fits after modeling the data. (a) Magnetic moment isotherms of **1**, fits obtained with $J_1 = -2.2$ K, $J_2 = -1.1$ K, and $J_3 = -0.1$ K. (Inset) The intramolecular exchange interactions are visualized in the distorted $[Mn_4O_4]$ core. The radii of the rods that connect the manganese ions give the strength of the magnetic exchange interactions. (b) Magnetic moment isotherms of **2**, fits obtained with $J_1 = -1.9$ K, $J_2 = -0.1$ K, and $J_3 = +0.2$ K. (c) Magnetic moment isotherms of **3**, fits obtained with $J_1 = -0.6$ K, $J_2 = -0.3$ K, and $J_3 = +0.1$ K.

temperatures, a behavior that is typical for a molecular magnet dominated by antiferromagnetic inter-ion exchange. The clusters start off in a nonmagnetic $S = 0$ ground state at low fields and saturate in an $S = 10$ state at high fields, where the Zeeman energy of each individual manganese ion in the cluster dominates the antiferromagnetic interactions between them. All 20 unpaired electrons in the Mn_4 cluster then have their spins aligned parallel to the magnetic field.

Key differences between the magnetic properties of our three types of Mn_4 clusters are visualized in their low-temperature magnetic-moment isotherms displayed in Figure 3. The acetate-bridged cluster, **1**, has the largest intramolecular antiferromagnetic interactions, resulting in the smallest slope at low magnetic fields. When electron density is withdrawn from the $[Mn_4O_4]$ core by the benzoate ligands in **2**, this coupling is decreased, as demonstrated in the increased slope. Even stronger electron density withdrawal by the trifluoroacetate ligands in **3** results in a largely increased slope at low magnetic fields, which approaches the magnetization behavior of

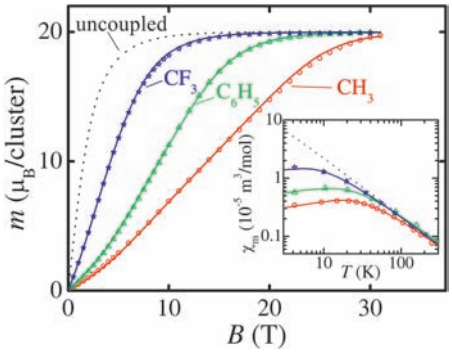

Figure 3. Overview of the magnetization and molar magnetic susceptibilities of the manganese clusters at low temperatures. Magnetic moment of **1** (○), **2** (△), and **3** (★) at 4.2 K. For comparison, the magnetic moment of four fully decoupled $S = 5/2$ Brillouin paramagnets is also shown (□). (Inset) Temperature dependencies of the molar magnetic susceptibilities of the Mn_4 clusters, extracted from the magnetic moment data at low magnetic fields, and the calculated paramagnetic susceptibility of four uncoupled $S = 5/2$ Brillouin paramagnets per cluster. Increasing the electron density withdrawal from the $[Mn_4O_4]$ core yields susceptibility curves that approach more and more that of a Brillouin paramagnet.

four independent $S = 5/2$ Brillouin paramagnets per cluster, in which no antiferromagnetic interactions are present at all.

The antiferromagnetic character of the Mn_4 clusters can also be observed in their low-field molar susceptibilities. For **1**, χ_1 gradually increases from low temperatures through the Néel point (inflection point) to a maximum and continues with inverse temperature behavior toward higher temperatures (see inset in Figure 3). The molar susceptibility of **3**, χ_3, hints toward a considerably smaller magnetic inter-ion coupling; it has no maximum within the measured temperature range. Its absolute value, however, still falls below the value expected for an uncoupled system of four $S = 5/2$ Brillouin paramagnets, indicating that some net antiferromagnetic interaction is still present in the trifluoroacetate-bridged Mn_4 cluster. Finally, the susceptibility of **2**, χ_2, falls between that of **1** and **3**, positioning its antiferromagnetic inter-ion coupling between the values for these two compounds.

Both the isothermal magnetic-moment measurements and the derived molar susceptibility show that changing the carboxylate ligands of the Mn_4 cluster from acetate to benzoate and trifluoroacetate decreases the antiferromagnetic intramolecular coupling. Therefore, we can already conclude that increasing the electron-withdrawing strength of the bridging ligands affects the orbital overlap of the $[Mn_4O_4]$ core such that these exchange interactions are decreased. Since our ligand variation only results in minor changes to the crystal structures, all differences in the magnetic behavior can be related to altered electron withdrawal by the ligands. The typical intermolecular distance in our clusters is about 8 Å. Hence, intermolecular magnetic couplings make a negligible contribution to the measured magnetic interactions, and only intramolecular interactions have to be taken into account in our detailed analysis.

Theoretical Calculations. For a more quantitative analysis of the measured magnetization data in terms of exchange interactions between the manganese ions, we have performed density functional theory (DFT) calculations where we evaluate the electronic structures of the

strongest and weakest antiferromagnetically coupled Mn_4 clusters **1** and **3** using the LDA+U method realized in the ASA-LMTO code Stuttgart-47.[15−18] We have used the same parameters as described in more detail in previous work and have based the value of the Coulomb repulsion in the calculation of the density of states (DOS), $U = 6$ eV, on the distance between the manganese 3d bands and the 2p bands of the oxygens in the cubane-like cores.[19−21] The resulting electronic structures of the clusters are shown in Figure 4a,b and agree well with previous experimental and theoretical results for other manganese-based SMMs.[22,23] Such broadened Mn 3d bands in the calculated spectra have also been experimentally observed in a Mn_6 cluster and a Mn_{12} cluster with aromatic ligands. The overlap of the Mn 3d bands and both O 2p bands indicates that all oxygens contribute to the magnetic exchange interactions. As noted above, the value of the exchange interaction depends on the overlap of the occupied electronic orbitals of the magnetic ions. Exchanging the acetate ligands by more electron-withdrawing trifluoroacetates moves the Mn 3d band lower on the energy scale, thereby changing the overlap such that the intramolecular magnetic exchanges between the manganese ions are decreased.

Next, we have used the obtained DOS results to calculate the exchange interactions between the four manganese ions using the magnetic force theorem, which varies the total energy at small spin rotations.[24] On the basis of the clusters' symmetry, three different exchange interaction pathways can be identified (see Figure 1c): an interplane interaction J_1 between nonequivalent carboxylate chelated Mn atoms (B or D) bridged only via the phenolate oxygen atoms (O_{Ph}) to the Mn atoms bound to an L^{2-} ligand (C or A) with Mn−O_{Ph}−Mn angles of ∼103−105°, an in-plane interaction J_2 over the carboxylate-bridged Mn atoms A−B and C−D with Mn−O_{Ph}−Mn angles of ∼90−94°, and the interplane interaction J_3 between two sets of equivalent ions (A−C and B−D). The calculations yield relatively large interplane antiferromagnetic exchange interactions J_1 (J_1 = −3 K for **1** and J_1 = −1 K for **3**); the in-plane antiferromagnetic exchange couplings J_2 are smaller than J_1 (J_2 = −1.5 K for **1** and J_2 = −0.5 K for **3**). Finally, the interplane exchange interaction constants between equivalent Mn ions show a small ferromagnetic coupling ($J_3 < 0.5$ K for both clusters). These calculations confirm both the experimental results where the magnetic moment of **3** increases much faster than that of **1** and the DFT results with increased Mn−O overlap for **3** and thus a weakened inter-ion coupling.

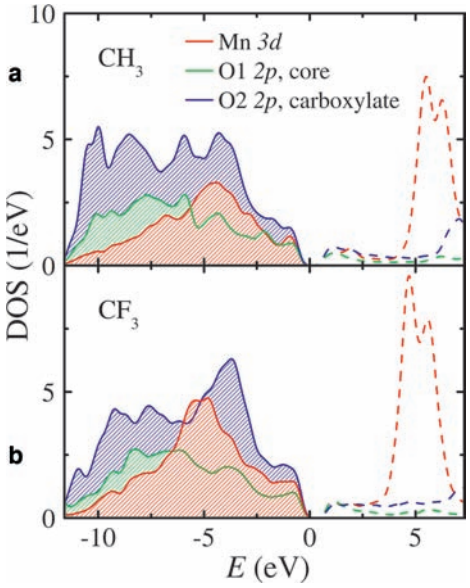

Figure 4. DFT calculations of the density of states. (a) The densities of the manganese 3d (red) and oxygen 2p states of **1** obtained from DFT calculations. The oxygens are divided into two groups: O1 (green) are oxygens between the manganese ions in the cubane core; O2 (blue) connect the manganese ions with the carboxylate ligands. The 2 eV distance between the main peaks of the Mn spectrum (located at −4 eV) and the O1 spectrum (located at −6 eV) is typical for a SMM electronic structure. (b) The main peak of the Mn spectrum in the DOS of **2** is clearly shifted toward lower energies, thereby changing the overlap of the electronic orbitals, resulting in decreased antiferromagnetic exchange interactions.

Discussion

Since DFT tends to overestimate the values for exchange constants, we have additionally fit our measured magnetic moment isotherms using the program julX.[25,26] For this, the large range of magnetic fields and temperatures used in our experiments is crucial to produce a reliable combination of parameters exactly fitting the measurements. On the basis of the clusters' symmetry and the DFT results, we use three independent exchange interaction constants as fit parameters: J_1, J_2, and J_3 as defined above. In order to obtain the magnetization as a function of magnetic field and temperature, julX solves the spin Hamiltonian: $\hat{H} = -2J_1(\hat{S}_A\hat{S}_D + \hat{S}_B\hat{S}_C) - 2J_2(\hat{S}_A\hat{S}_B + \hat{S}_C\hat{S}_D) - 2J_3(\hat{S}_A\hat{S}_C + \hat{S}_B\hat{S}_D) + \sum_i^{ns} g\mu_B\hat{S}_i\hat{B}$ via numerical matrix diagonalization. Since our clusters consist of four isotropic Mn^{II} ions with a nonmagnetic $S = 0$ ground state, no anisotropy or zero-field splitting terms are used. A correction for the diamagnetic background was determined by taking the difference of the high-temperature magnetic-moment isotherms and the theoretical Brillouin function. The solid lines in Figure 2a show

(15) Anisimov, V. I.; Zaanen, J.; Andersen, O. K. *Phys. Rev. B* **1991**, *44*, 943.
(16) Anisimov, V. I.; Aryasetiawan, F.; Lichtenstein, A. I. *J. Phys.: Condens. Matter* **1997**, *9*, 767.
(17) Andersen, O. K. *Phys. Rev. B* **1975**, *12*, 3060.
(18) Andersen, O. K.; Jepsen, O. *Phys. Rev. Lett.* **1984**, *53*, 2571.
(19) Boukhvalov, D. W.; Al-Saqer, M.; Kurmaev, E. Z.; Moewes, A.; Galakhov, V. R.; Finkelstein, L. D.; Chiuzbaian, S.; Neumann, M.; Dobrovitski, V. V.; Katsnelson, M. I.; Lichtenstein, A. I.; Harmon, B. N.; Endo, K.; North, J. M.; Dalal, N. S. *Phys. Rev. B* **2007**, *75*, 014419.
(20) Boukhvalov, D. W.; Dobrovitski, V. V.; Katsnelson, M. I.; Lichtenstein, A. I.; Harmon, B. N.; Kogerler, P. *Phys. Rev. B* **2004**, *70*, 054417.
(21) Barbour, A.; Luttrell, R. D.; Choi, J.; Musfeldt, J. L.; Zipse, D.; Dalal, N. S.; Boukhvalov, D. W.; Dobrovitski, V. V.; Katsnelson, M. I.; Lichtenstein, A. I.; Harmon, B. N.; Kogerler, P. *Phys. Rev. B* **2006**, *74*, 014411.
(22) Voss, S.; Fonin, M.; Rudiger, U.; Burgert, M.; Groth, U.; Dedkov, Y. S. *Phys. Rev. B* **2007**, *75*, 045102.
(23) del Pennino, U.; Corradini, V.; Biagi, R.; De Renzi, V.; Moro, F.; Boukhvalov, D. W.; Panaccione, G.; Hochstrasser, M.; Carbone, C.; Milios, C. J.; Brechin, E. K. *Phys. Rev. B* **2008**, *77*, 085419.
(24) Liechtenstein, A. I.; Katsnelson, M. I.; Antropov, V. P.; Gubanov, V. A. *J. Magn. Magn. Mater.* **1987**, *67*, 65.
(25) Voss, S.; Fonin, M.; Rudiger, U.; Burgert, M.; Groth, U. *Appl. Phys. Lett.* **2007**, *90*, 133104.
(26) Available at http://ewww.mpi-muelheim.mpg.de/bac/logins/bill/julX_en.php (accessed Nov 2009).

the best fits to the model for sample **1** with exchange interaction constants $J_1 = -2.2$ K, $J_2 = -1.1$ K, and J_3 −0.1 K. These values are comparable to earlier studies on molecules containing analogous $[Mn^{II}{}_4O_4]$ cores with weak antiferromagnetic interactions within the range of +0.4 to −5.9 K.[27,28] There is good quantitative agreement with the DFT results, with two main antiferromagnetic interactions and negligible coupling between the equivalent manganese ions. The results for **2** (solid lines in Figure 2b) give interaction constants $J_1 = -1.9$ K, $J_2 = -0.1$ K, and $J_3 = +0.2$ K. Thus, the antiferromagnetic couplings J_1 and J_2 have markedly decreased on going from the acetate-bridged cluster **1** to the benzoate-bridged cluster **2**. The fits for **3** in Figure 2c yield exchange interaction constants $J_1 = -0.6$ K, $J_2 = -0.3$ K, and $J_3 = +0.1$ K. Again the antiferromagnetic couplings J_1 and J_2 have decreased with respect to **1**. As in **2**, the small coupling constant J_3 changed from antiferromagnetic to ferromagnetic but remains small and is thus unable to overcome the larger antiferromagnetic interactions that make the magnetic moment saturate at high magnetic fields.

We thus safely assign the exchange interactions of cluster **1** being dominated by two mainly antiferromagnetic interactions J_1 and J_2 between the nonequivalent manganese ions, while the J_3 couplings between the equivalent manganese ions are small. The coupling scheme of **2** is similar to that of **1** with reduced values for the large antiferromagnetic exchange constants due to the increased electron-withdrawing character of the benzoate ligands. Cluster **3** shows the same decreasing trend for the antiferromagnetic couplings J_1 and J_2. The tendency of J_3 to evolve toward a ferromagnetic interaction shows the electron density withdrawing effect of the benzoate and trifluoroacetate ligands with respect to the acetates but is yet too small to have a clear effect on the magnetic character of the cluster.

Conclusions

In conclusion, we have synthesized a new type of manganese cluster with a distorted cubane-like $[Mn_4O_4]$ core, in which the carboxylate ligands that bridge the manganese ions determine their electronic orbital overlap and therefore the strength of the magnetic exchange interactions between them. On the basis of DFT calculations and experimentally measured magnetic moment isotherms, we were able to quantify these exchange parameters with three independent exchange constants. Interchanging the ligands from acetate to benzoate and trifluoroacetate increased the electron-withdrawing capacity and made it possible to reduce the strong antiferromagnetic interactions and induce small ferromagnetic interactions instead. Our results constitute a new starting point for user-designed molecular magnets, where magnetic properties can be predicted and controlled through the electron-withdrawing character of the interchangeable ligands.

Experimental Section

General Considerations. Reagents were purchased from commercial suppliers and used as-received. The elemental analyses were carried out by the Analytische Laboratorien in Lindlar, Germany.

X-Ray Diffraction Studies. Single-crystal diffraction was performed on a Nonius KappaCCD single-crystal diffractometer (φ and ω scan mode) using graphite monochromated Mo Kα radiation. Intensity data were corrected for Lorentz and polarization effects. A semiempirical multiscan absorption correction was applied (SADABS).[29] The structures were solved by the DIRDIF program system using the program PATTY to locate the heavy atoms. Refinement was performed with standard methods (refinement against F^2 of all reflections with SHELXL97) with anisotropic displacement parameters for the non-hydrogen atoms, except for the solvent molecules in the structure of compound **3**.[30,31] All hydrogen atoms were placed at calculated positions and refined riding on the parent atoms.

For compound **3**, several crystals from different batches were measured, with the best data presented in this work. The electron density map showed the presence of three solvent molecules. One of the THF solvent molecules could be described isotropically, and for the other solvent residues, the program SQUEEZE was used. The number of electrons that was found was unreliable due to the absence of important low-order reflections. However, it is evident from the difference map that the solvent residues consist of THF and diethyl ether with a partial occupation. This is in agreement with the elemental analysis of **3**, from which we know that the occupancy factor is about 0.5 for each molecule, leading to a ratio of Mn_4 cluster/THF/Et_2O of 2:3:1.

Crystal data for **1**: translucent red-brown, $C_{59}H_{67}N_9O_{15}Mn_4$, $M = 1361.98$, monoclinic, space group $P21/c$, $a = 11.4395(14)$, $b = 19.923(4)$, $c = 27.660(5)$ Å, $\alpha = 90$, $\beta = 101.527(10)$, $\gamma = 90°$, $V = 6177.0(17)$ Å^3, $T = 208(2)$ K, $Z = 4$, 87 755 reflections measured, 14 010 unique ($R_{int} = 0.0375$), final $R_1 = 0.0521$, final $wR_2 = 0.1014$ ($I > 2\sigma(I)$), GOF on $F^2 = 1.150$.

Crystal data for **3**: translucent red-brown, $C_{54}H_{42}N_6O_{13}F_{12}Mn_4$, $M = 1430.70$, monoclinic, space group $P21/n$, $a = 18.524(3)$, $b = 19.288(4)$, $c = 19.418(2)$ Å, $\alpha = 90$, $\beta = 106.242(10)$, $\gamma = 90°$, $V = 6661.4(18)$ Å^3, $T = 208(2)$ K, $Z = 4$, 34 128 reflections measured, 9327 unique ($R_{int} = 0.0613$), final $R_1 = 0.0749$, final $wR_2 = 0.1924$ ($I > 2\sigma(I)$), GOF on $F^2 = 0.976$.

Magnetometry. Magnetic moments were measured with an extraction magnetometer at various temperatures ($T = 4$ ... 300 K) using a flow cryostat in DC magnetic fields up to 31 T, available at the High Field Magnet Laboratory (HFML) in Nijmegen.[32,33]

Mn_4[2,6-bis(1-(2-hydroxyphenyl)iminoethyl)pyridine]$_2$[acetate]$_4$ (1). A mixture of 2.00 g of 2,6-diacetylpyridine (12.3 mmol), 2.68 g of 2-aminophenol (24.7 mmol), and 6.00 g of $Mn(OAc)_2 \cdot 4H_2O$ (24.7 mmol) was refluxed in 100 mL of methanol for 2 h. The deep red solution was allowed to cool to room temperature, causing the precipitation of microcrystalline red Mn_4[2,6-bis(1-(2-hydroxyphenyl)-iminoethyl)-pyridine]$_2$[acetate]$_4$ (2.77 g, 40%). Recrystallization from dmf top-layered with pentane afforded deep red-black cubic crystals, identified as **1** · 3dmf. Elem anal. (%) calcd for $Mn_4L_2[H_3CCOO]_4 \cdot 3$dmf ($C_{59}H_{67}N_9O_{15}Mn_4$): C, 52.03; H, 4.96; N, 9.26. Found: C, 51.91; H, 4.94; N, 9.23.

$Mn(H_5C_6COO)_2 \cdot 2H_2O$. To a solution of 14.6 g of sodium benzoate (0.1 mol) in 75 mL of H_2O at 80 °C was added a

(27) Brooker, S.; McKee, V.; Shepard, W. B.; Pannell, L. K. *J. Chem. Soc., Dalton Trans.* **1987**, 2555.
(28) Aussoleil, J.; Cassoux, P.; Deloth, P.; Tuchagues, J. P. *Inorg. Chem.* **1989**, *28*, 3051.
(29) Sheldrick, G. M. *SADABS*; Universität Göttingen: Göttingen, Germany, 1996.
(30) Beurskens, P. T.; Admiraal, G.; Beurskens, G.; Bosman, W. P.; de Gelder, R.; Israël, R.; Smits, J. M. M. *The DIRDIF Program System, Technical Report of the Crystallography Laboratory*, University of Nijmegen, Nijmegen, The Netherlands, 1997.
(31) Sheldrick, G. M. *SHELXL-97*; Universität Göttingen: Göttingen, Germany, 1997.
(32) Foner, S.; Mcniff, E. J. *Rev. Sci. Instrum.* **1968**, *39*, 171.
(33) Perenboom, J.; Wiegers, S. A. J.; Christianen, P. C. M.; Zeitler, U.; Maan, J. C. *J. Low Temp. Phys.* **2003**, *133*, 181.

solution of 10.0 g o f$MnCl_2 \cdot 4H_2O$ (0.05 mol) in 50 mL of H_2O. The solution was vigorously stirred for 10 min at 80 °C. After cooling to room tmeperature, the pink precipitate was isolated. Elem anal. (%) calcd for $Mn[H_5C_6COO] \cdot 2H_2O$ ($C_{14}H_{14}O_6Mn$): C, 50.47; H, 4.24. Found: C, 50.23; H, 4.15.

Mn_4[2,6-bis(1-(2-hydroxyphenyl)iminoethyl)pyridine]$_2$[benzoate]$_4$ (2). A solution of 2.0 g of $Mn(H_5C_6COO)_2 \cdot 2H_2O$ (6 mmol), 0.490 g of diacetylpyridine (3 mmol), and 0.655 g of aminophenol (6 mmol) in 100 mL of MeOH was refluxed for 3 h under an inert atmosphere. After cooling down to room temperature, a red precipitate was isolated. Elem anal. (%) calcd for $Mn_4L_2[H_5C_6COO]_4 \cdot 3.5MeOH \cdot 1.5H_2O$ ($C_{73.5}H_{60.5}N_6O_{17}Mn_4$): C, 57.69; H, 4.68; N, 5.49. Found: C, 57.33; H, 4.53; N, 5.73

Mn_4[2,6-bis(1-(2-hydroxyphenyl)iminoethyl)pyridine]$_2$[F_3CCOO]$_4$ (3). To a solution of 300 mg of **1** (0.26 mmol) in 30 mL of MeOH was added a solution of 150 mg of trifluoroacetic acid (5 equiv, 1.3 mmol) in 10 mL of MeOH. After stirring for 45 min, the solvent was removed, and the residue was dissolved into a methanol/toluene mixture (1:3). By re-evaporating the solvent, the remaining acetic acid and TFA were removed. Single crystals were obtained via diffusion of Et_2O into a THF solution of the crude material. Elem anal. (%) calcd for $Mn_4L_2[F_3CCOO]_4 \cdot 1.5THF \cdot 0.5Et_2O$ ($C_{58}H_{51}N_6O_{14}F_{12}Mn_4$): C, 46.32; H, 3.42; N, 5.59; F, 15.16, M_n, 14.61. Found: C, 46.12; H, 3.48; N, 5.82; F, 15.56; M_n, 14.36.

Acknowledgment. This work has been supported by the Stichting Fundamenteel Onderzoek der Materie (FOM) with financial support from the Nederlandse Organisatie voor Wetenschappelijk Onderzoek (NWO). We thank Paul Schlebos for his contributions to the synthesis of the Mn_4 clusters, Hung van Luong for the development of the extraction magnetometer and his help during the magnetization experiments, and Eckhard Bill for his help with modeling the data with julX.

Note Added after ASAP Publication. This article was released ASAP on November 16, 2009, with minor errors in Figure 1. The correct version was posted on November 19, 2009.

Supporting Information Available: X-ray crystallographic data in the form of a crystallographic information file (CIF) for clusters **1** and **3**. This material is available free of charge via the Internet at http://pubs.acs.org.